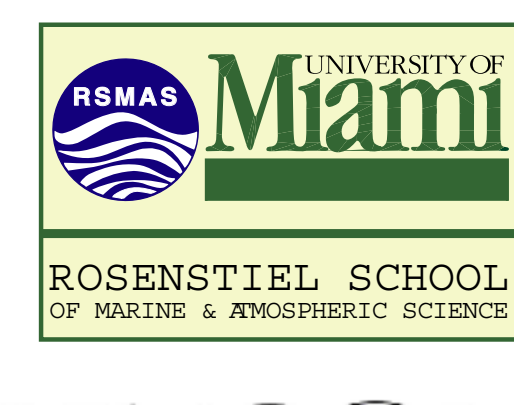


North Atlantic Simulations with the HYbrid Coordinate Ocean Model (HYCOM): Impact of the Vertical Coordinate Choice, Reference Density, and Thermobaricity



Eric P. Chassignet¹, Linda T. Smith¹, George R. Halliwell¹, and Rainer Bleck²

¹ (RSMAS/UM) Rosenstiel School of Marine and Atmospheric Science, University of Miami, Miami, FL ² Los Alamos National Laboratory, Los Alamos, New Mexico

BACKGROUND

Previous MICOM experiments for the North and Equatorial Atlantic basin in the CME configuration, 0.9° horizontal resolution, Kraus - Turner mixed layer + 15 isopycnic layers (σ_θ coordinate). (Chassignet et al., JPO, 1996; Smith et al., JPO, 2000).

Comparison of MICOM experiments to GFDL depth - coordinate model experiments in the CME configuration (Bryan and Holland, Proceedings, 1989). Other comparisons of North and Equatorial Atlantic models in depth or density coordinates (Roberts et al., JPO, 1996; Marsh et al., JPO, 1996).

Model comparison exercises focusing on the choice of vertical coordinate -- depth, density, or the terrain-following sigma. (Dynamics of North Atlantic Models -- DYNAMO, Willebrand et al., Prog. Oceanogr., 2001; Data Assimilation and Model Evaluation Experiment - DAMEE, Chassignet et al., Dyn. Atmos. Oceans, 2000) showed that there is no single optimal vertical coordinate choice.

MOTIVATION

To utilize the built-in vertical coordinate flexibility of the generalized coordinate (hybrid) model, HYCOM, to assess the importance of the vertical coordinate choice, reference density, and thermobaricity on the model's ability to accurately represent the water mass distributions and three-dimensional circulation of the Atlantic. The emphasis is on

– the vertical coordinate choice: hybrid, isopycnic, pressure-level

– the coordinate representation and reference density: σ_θ , σ_2 , σ_2^* with correction for thermobaricity, Sun et al., JPO, 1999.

– the mixed-layer parameterization: Kraus-Turner (K-T), Kraus and Turner, 1967; K-Profile Parameterization (KPP), Large et al., 1994, 1997.

MODEL CONFIGURATION

Model: HYCOM (Bleck, Ocean Modelling, 2002) <http://hycom.rsmas.miami.edu>

Basin: North and Equatorial Atlantic: 15° S - 65° N
0.9° (Mercator)

Topography: ETOP05 (1/12°)

Wind stress/wind work: Hellerman & Rosenstein (1983)

Surface thermal boundary conditions: Han (1984)

Fresh water flux boundary conditions: relaxation to Levitus (1982) surface salinity

Initial conditions: January Levitus (1982)

Buffer zones: relaxation to Levitus (1982) T, S in northern and southern boundary regions, Labrador shelf, Gulf of Cadiz

EXPERIMENTS & LAYER DENSITIES

experiment	coordinate	layers/levels	mixed layer
EXP-M', M	σ_θ	22	K-T
EXP-H _{KT}	σ_θ/p	22	K-T
EXP-H	σ_θ/p	22	KPP
EXP-H ₈₀	$\sim \sigma_\theta$	22	KPP
EXP-H _p	p	30	KPP
EXP-H σ_2	σ_2/p	22	KPP
EXP-H σ_2^*	σ_2^*/p	22	KPP

Layer	EXP-M', M, H _{KT} , H	EXP-H ₈₀	EXP-H _p , H σ_2^*
1	21.40	23.50	29.04
2	21.80	24.00	29.47
3	22.20	24.25	29.89
4	22.60	24.50	30.32
5	23.05	24.70	30.80
6	23.55	25.00	31.34
7	24.02	25.25	31.82
8	24.70	25.50	33.19
9	25.25	25.70	34.22
10	25.77	26.00	35.01
11	26.19	26.16	35.59
12	26.52	26.52	35.98
13	26.89	26.89	36.27
14	27.03	27.03	36.49
15	27.22	27.22	36.66
16	27.36	27.36	36.79
17	27.52	27.52	36.89
18	27.64	27.64	36.98
19	27.74	27.74	37.04
20	27.82	27.82	37.08
21	27.88	27.88	37.11
22	27.92	27.92	37.14

SURFACE CIRCULATION

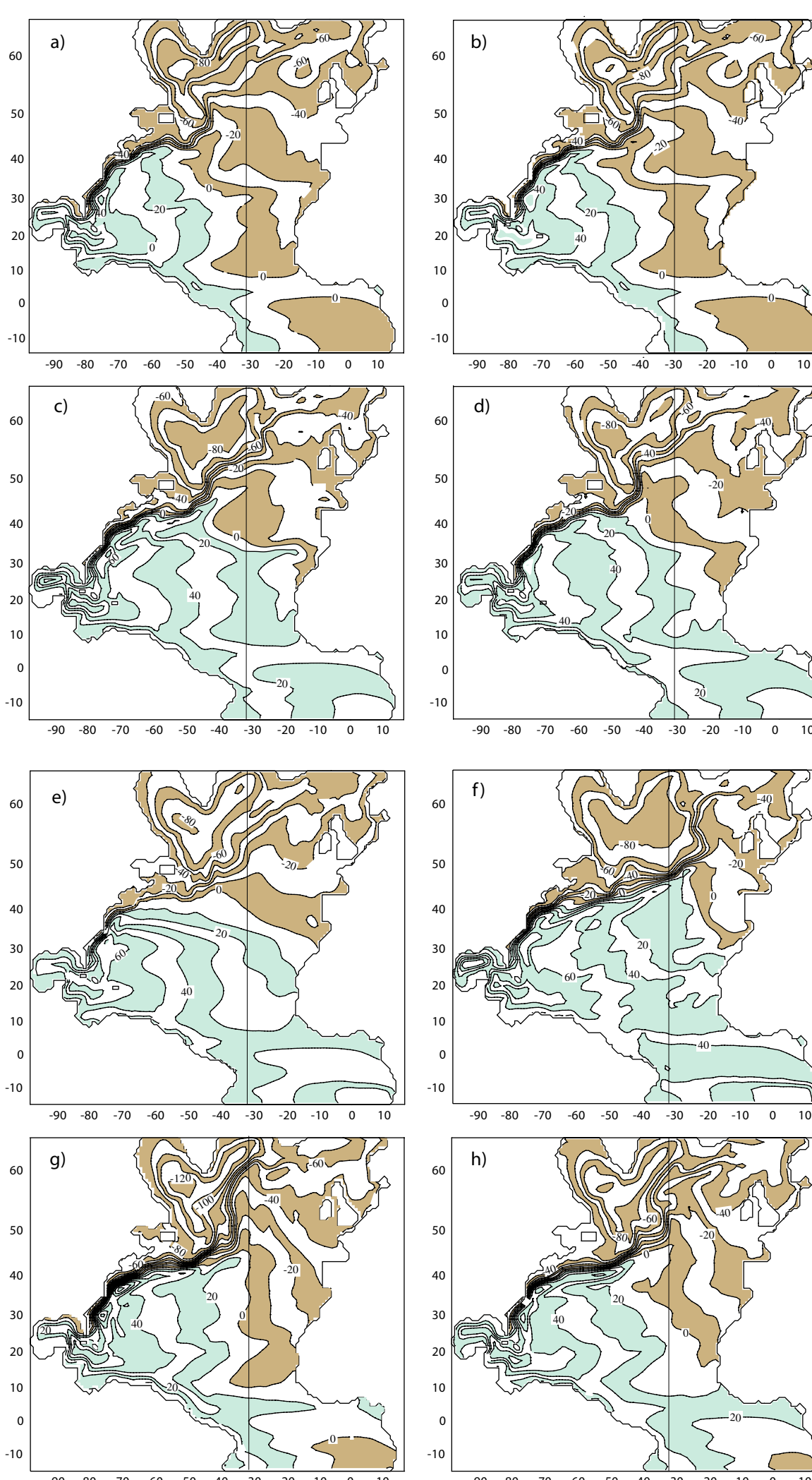


Fig. 1. Sea Surface Height (cm), mean years 18-20. Contour interval 10 cm. (a) EXP-M', (b) EXP-M, (c) EXP-HKT, (d) EXP-H, (e) EXP-Hp, (f) EXP-H80, (g) EXP-H σ_2 , (h) EXP-H σ_2^* . Vertical line along 31.8°W.

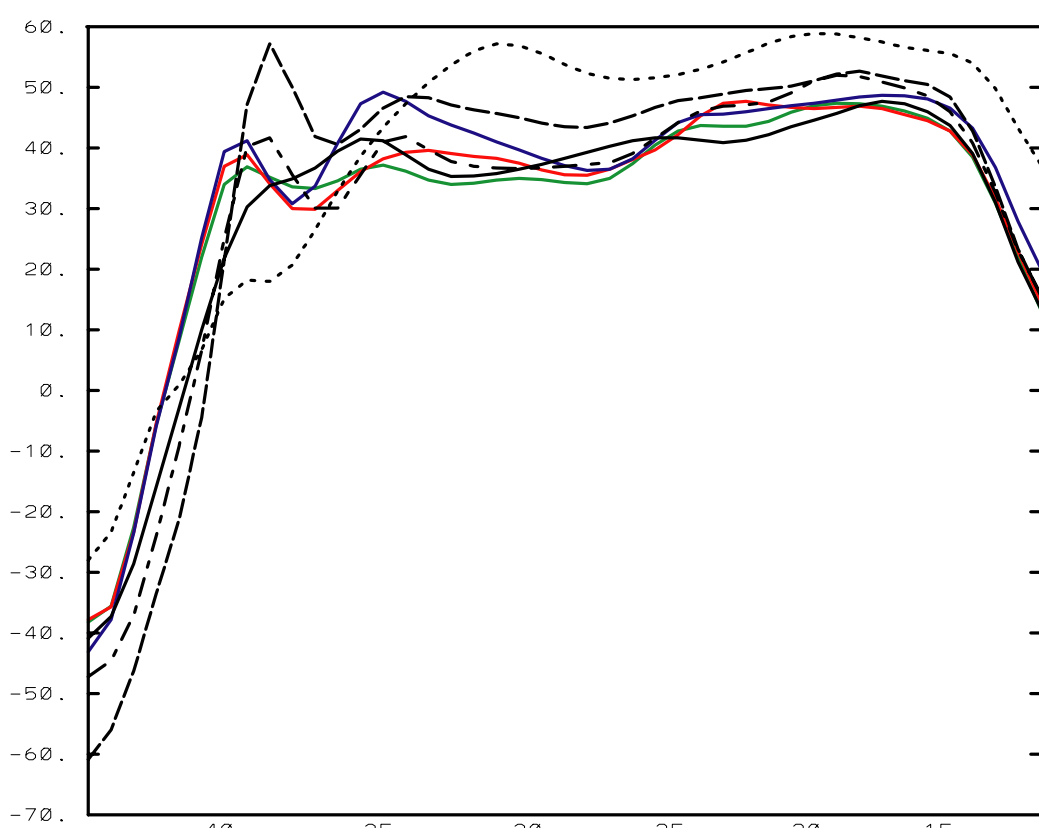


Fig. 2. Sea Surface Height (cm) along 65°W, mean years 18-20. Green: EXP-A; red: EXP-B; blue: EXP-C; black: EXP-D; long dash: EXP-E; dash-dot: EXP-F; dot: EXP-Dx.

SURFACE CIRCULATION

Strength of the circulation as measured by the SSH

- Most diffuse in EXP-Hp
- Strongest in EXP-H σ_2 , with inaccurate pressure gradients at surface
- Use of virtual potential density in EXP-H σ_2^* corrects for density variations caused by thermobaricity, so that surface pressure gradients are similar to those of σ_θ experiments M', H_{KT}, and H (Fig. 2)

Path of the North Atlantic Current

- Experiments with weaker subpolar gyres (M', M, H_{KT}, H, H_p) show NAC turning north at the Flemish Cap at 45°W before turning east between 50 and 55°N
- Subpolar gyre is intensified in EXP-H σ_2 ; NAC extends farther east (35°W) before turning north

- With thermobaricity (EXP-H σ_2^*), subpolar gyre strength is similar to that of experiments M', M, H_{KT}, H, and H_p; NAC branches out northward and northeastward at the Flemish Cap (45°W)

Sea Surface Height along 65°W

Weaker SSH gradient across Gulf Stream in EXP-H_p than in the hybrid and isopycnic experiments

Strongest SSH gradient across Gulf Stream in EXP-H σ_2

SSH gradient of EXP-H σ_2^* similar to that of the σ_θ experiments

CROSS-SECTIONS

VERTICAL CROSS-SECTIONS ALONG 31.8°W

Comparison of EXP-H and EXP-H_p to assess impact of hybrid coordinates vs. fixed coordinates

- Layer 22 water in EXP-H ($\sigma_\theta \sim 27.92$) has nearly disappeared in EXP-H_p after 20 years

Density gradients in EXP-H_p are weaker than in EXP-H. Fronts are better represented by hybrid and isopycnic coordinates than by pressure-level coordinates.

Comparison of EXP-H, EXP-H σ_2 , and EXP-H σ_2^* to assess impact of the reference pressure choice and the correction for thermobaricity

- Density front marking the NAC is well defined in the hybrid experiments by sharply rising isopycnals, but location of the front varies

In EXP-H σ_2 , relatively flat isopycnals from 50-55°N reflect the due north path of the NAC along 35°W; incorrect pressure gradients at the surface and absence of thermobaric effects lead to intensified subpolar gyre and NAC path that extends farther to the east

- EXP-H σ_2^* , with reference pressure at 20 MPa and thermobaric effects included, more closely resembles EXP-H, with reference pressure at the surface, in the region of the NAC eastward and northward turn, both here and in the SSH

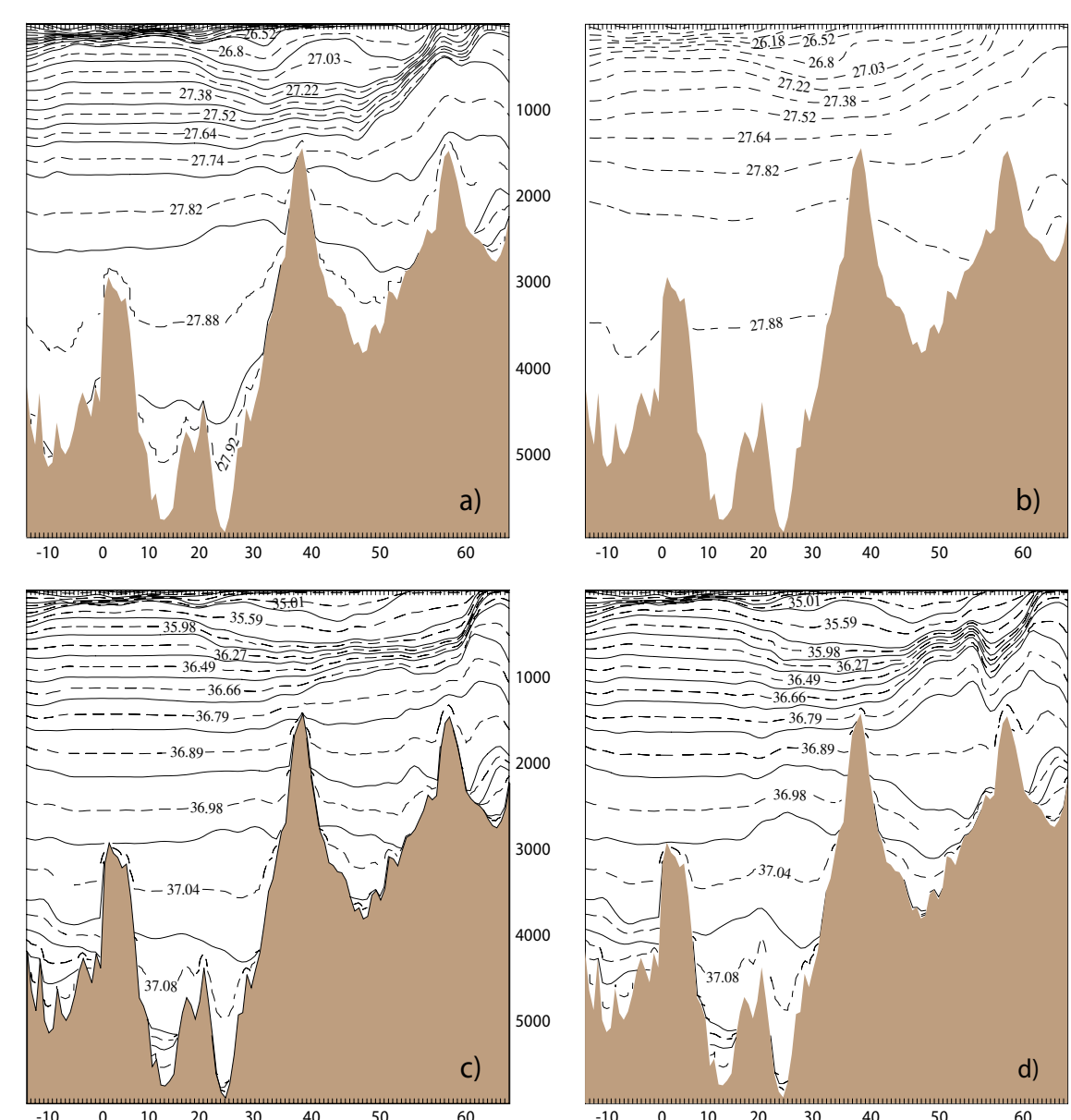


Fig. 4. Vertical cross-sections along 31.8°W, mean years 18-20. (a) EXP-H, (b) EXP-Hp, (c) EXP-H σ_2 , (d) EXP-H σ_2^* . Solid lines are layer interfaces for EXP-H, H σ_2 , H σ_2^* . Dashed lines show layer density (σ_0) for EXP-H, H_p; σ_2 for EXP-H σ_2 , H σ_2^* .

CROSS-SECTIONS IN EQUATORIAL REGION

Zonal velocity in the upper 250 m along 31.8°W from ~7°S - 7°N, for EXP-H, EXP-Hp, EXP-H σ_2^*

- Core EUC velocity is ~ 40 m/s in all 3 experiments

Increased vertical discretization in density is evident in hybrid experiments EXP-H and EXP-H σ_2 as compared to the fixed-coordinate EXP-Hp

Southern branch of the South Equatorial Current (SEC) is surface intensified in EXP-H and EXP-H σ_2 as compared to that of EXP-Hp, which lacks near-surface resolution

Zonal velocity in the upper 250 m along the equator, across the model basin, for EXP-H, EXP-Hp, EXP-H σ_2^*

- Increased vertical discretization in density again evident in hybrid experiments EXP-H and EXP-H σ_2 as compared to the fixed-coordinate EXP-Hp

Westward cross-equatorial flow associated with the North Brazil Current is not represented below 100 m in EXP-Hp, while cross-equatorial flow in EXP-H and EXP-H σ_2 extends to a depth of 250 m

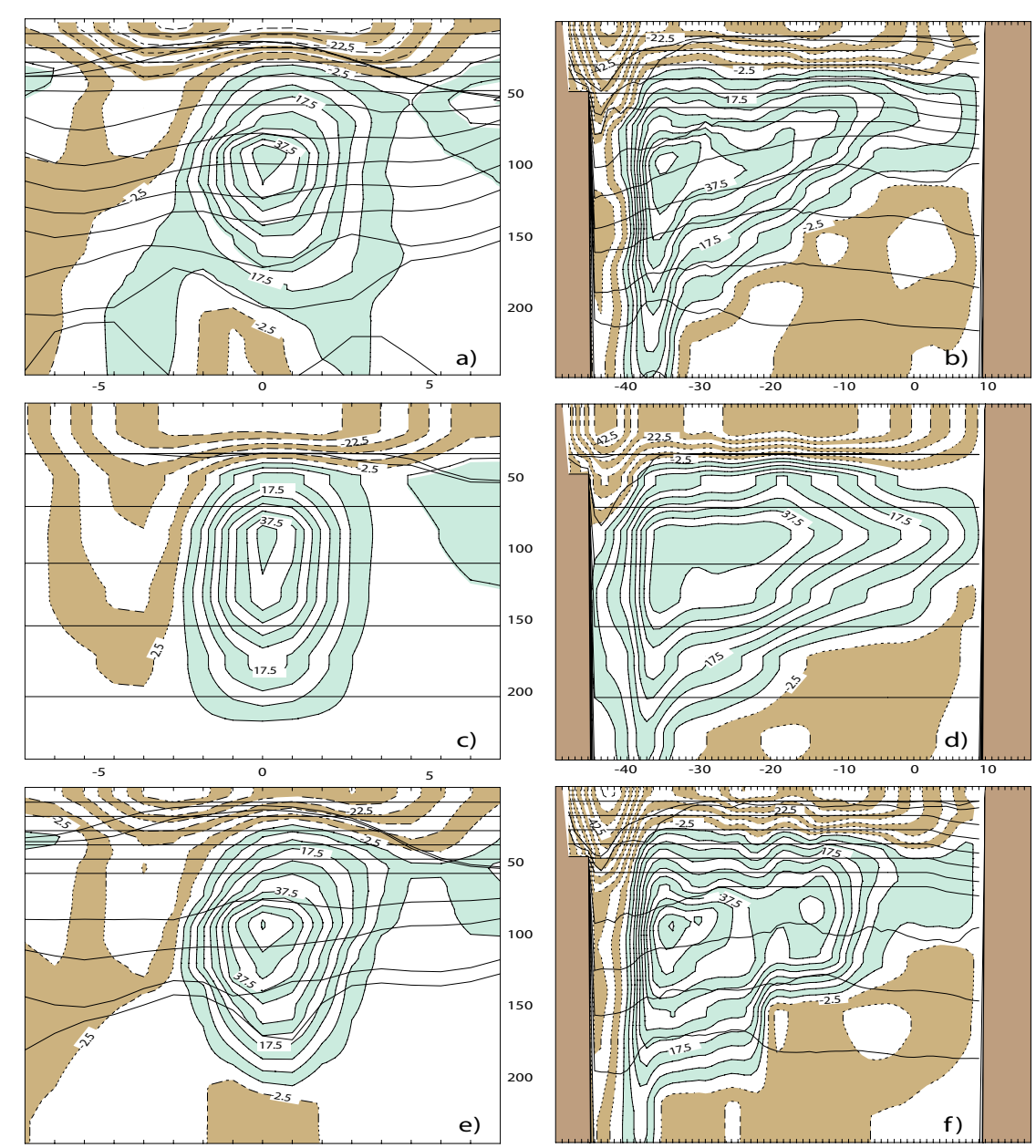


Fig. 6. Vertical cross-sections along 31.8°W from ~7°S - 7°N (left panels), and along the equator, across the model basin (right panels), for March year 20, showing contours of zonal velocity (contour interval 5 cm/sec). (a,b) EXP-H, (c,d) EXP-Hp, (e,f) EXP-H σ_2^* . Solid lines are layer interfaces. Integers are layer numbers. Depth shown in meters on vertical axis.

MIXED LAYER DEPTH

MIXED LAYER DEPTH

Deepest mixed layer over northern subtropical gyre found in the MICOM EXP-M and HYCOM EXP-H_{KT}, which use the bulk Kraus-Turner mixed layer

Winter mixed layer depth in Labrador Sea is shallowest in Kraus-Turner EXP-M and EXP-H_{KT}, deepest in KPP cases EXP-H, EXP-Hp, EXP-H σ_2 , and EXP-H σ_2^*

Large changes in mixed layer depths in weakly stratified regions result from small changes in temperature and salinity arising from different vertical discretizations (isopycnic, pressure-level, hybrid) and from different reference pressure choices

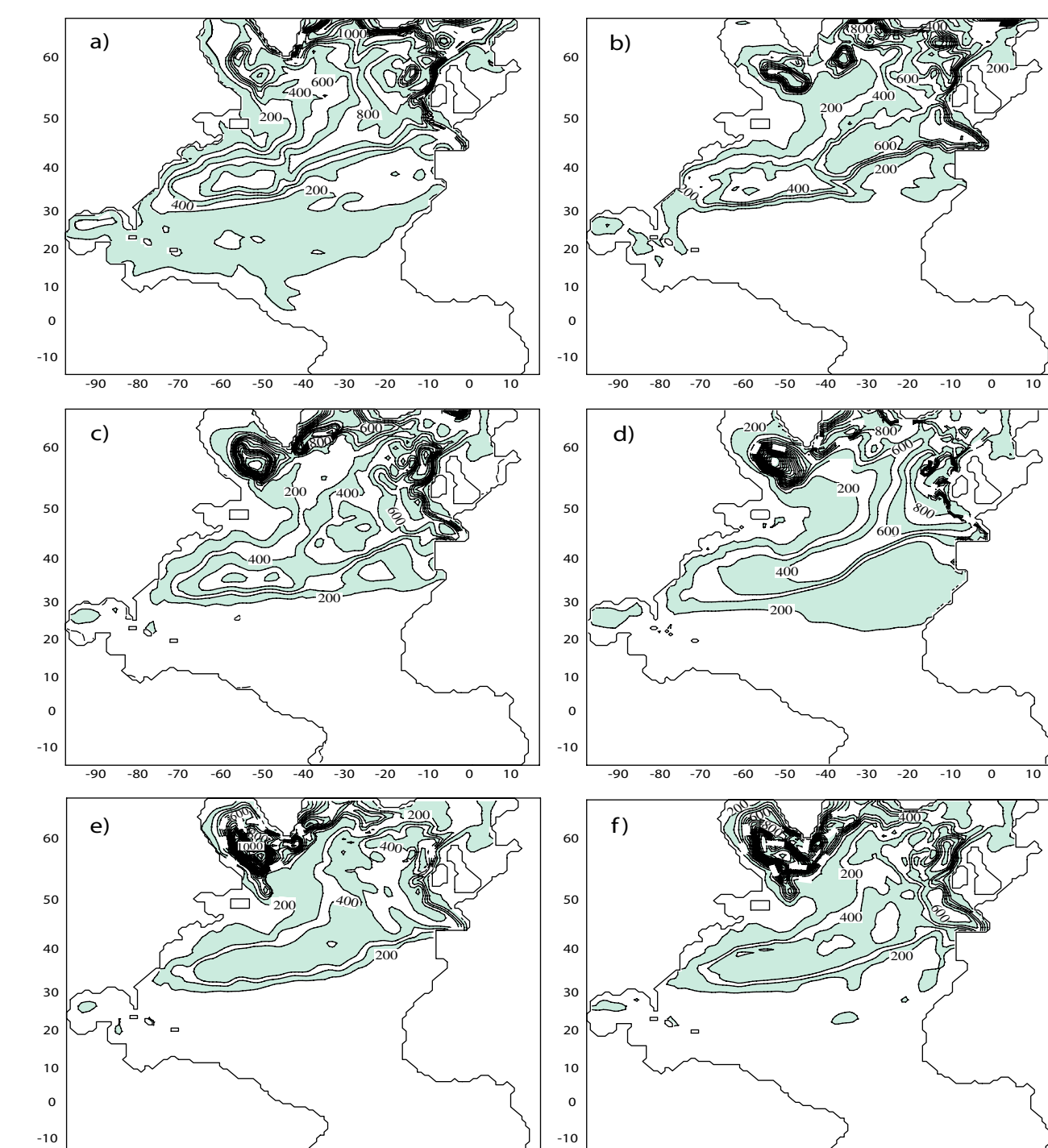


Fig. 3. Mixed layer depth (m), March mean years 18-20. Contour interval 100 m. (a) EXP-M, (b) EXP-HKT, (c) EXP-H, (d) EXP-Hp, (e) EXP-H σ_2 , (f) EXP-H σ_2^* .

DENSITY DIFFERENCE BETWEEN PAIRS OF EXPERIMENTS

Density difference between EXP-H σ_2 and EXP-H, shown in σ_θ space and in σ_2 space

- NAC carries warm water to latitudes north of 55°N along this longitude in EXP-H σ_2 , while in EXP-H, the NAC turns north at a point farther west and then turns sharply to the east, carrying less heat to higher latitudes

From 25-50°N, denser water is present between 500 and 1000 m in EXP-H σ_2 , relative to EXP-H, due to the deeper subtropical gyre thermocline of EXP-H

- Water below ~2000 m appearing heavier in EXP-H σ_2 relative to EXP-H when viewed in σ_2 (and the opposite when viewed in σ_θ) arises from the different initial conditions between the two experiments

Density difference between EXP-H σ_2^* and EXP-H σ_2 shown in σ_2 space

- Differences between EXP-H σ_2^* and EXP-H σ_2 are largest in the representation of the NAC and below 2000 m

- Differences are due to inclusion of thermobaric effects in EXP-H σ_2^* , and are expected in regions of steep density gradients and at depths where AABW flows northward

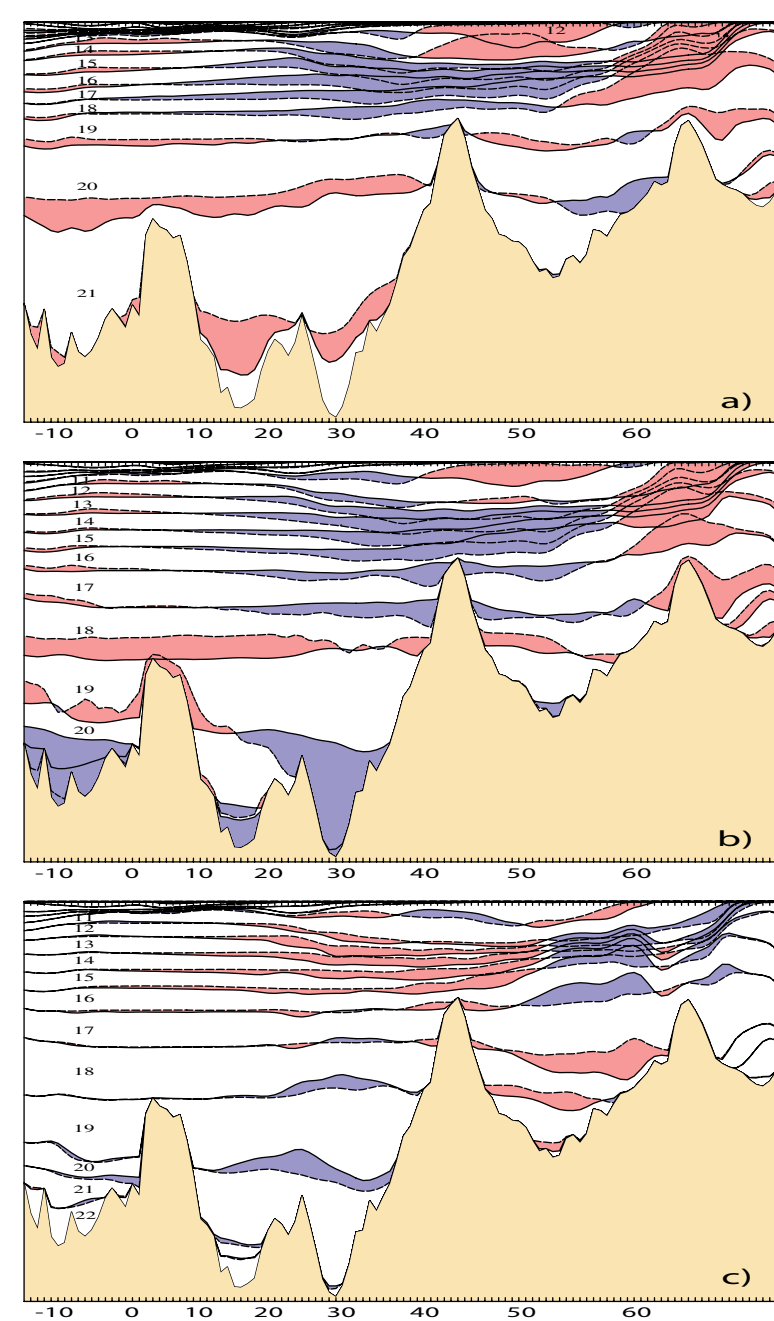


Fig. 5. Vertical cross-sections along 31.8°W, mean years 18-20, showing density difference between two experiments. (a) EXP-H σ_2 -EXP-H, displayed in σ_θ . (b) EXP-H σ_2 -EXP-H, displayed in σ_2 . (c) EXP-H σ_2 -EXP-H σ_2^* , displayed in σ_2 . Red (blue) shading indicates first experiment is lighter (heavier) than second experiment.

CENSUS

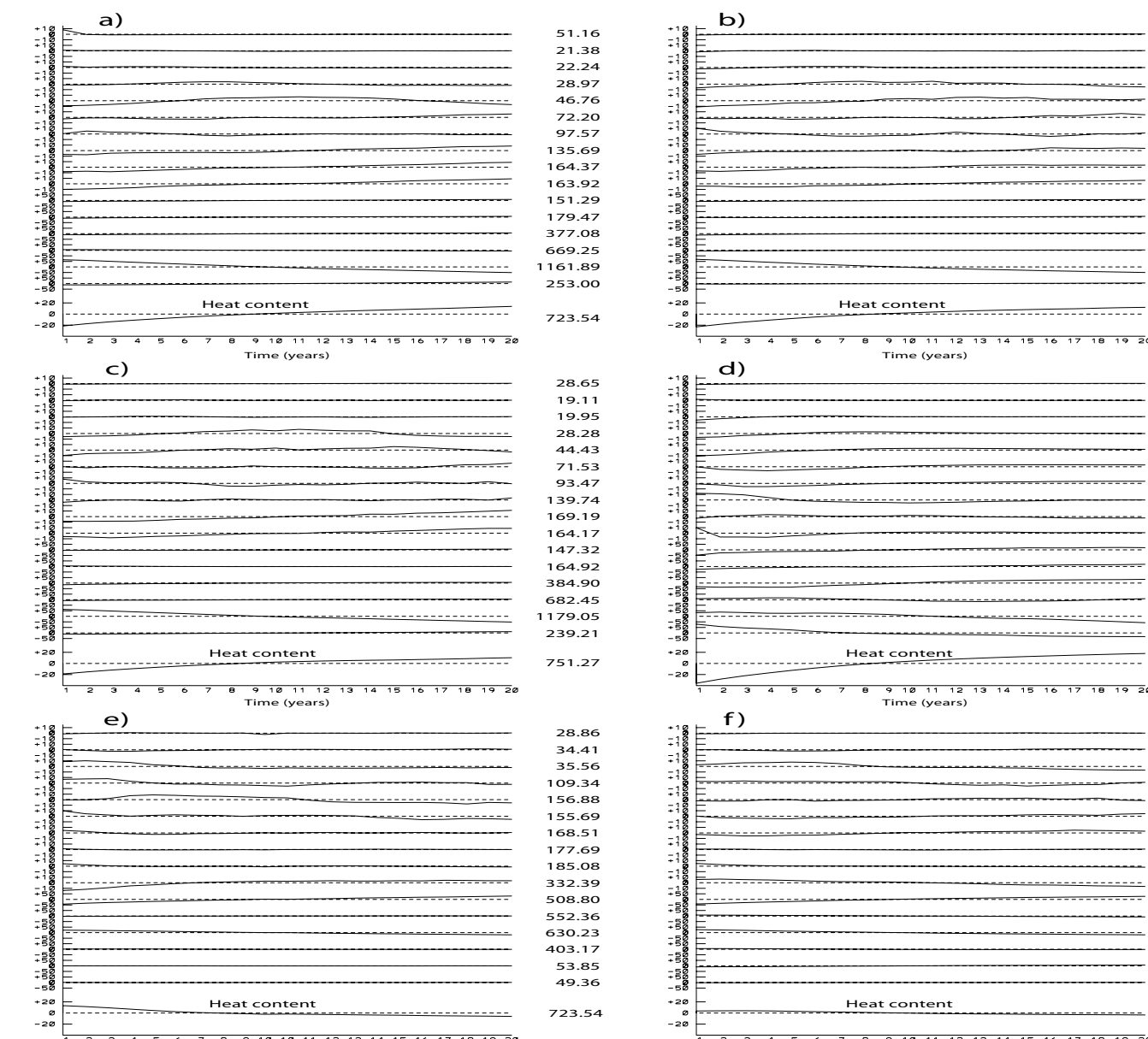


Fig. 7. 20-year time evolution of the domain-averaged layer thicknesses in meters for 16 heaviest coordinate density classes, and of the domain-averaged heat content (bottom curve), computed for the month of September for (a) EXP-M, (b) EXP-HKT, (c) EXP-H, (d) EXP-Hp, (e) EXP-H σ_2 , (f) EXP-H σ_2^* . Basin-mean time-mean thickness and heat content values shown at right.

CENSUS

σ_θ experiments: EXP-M, EXP-H_{KT}, EXP-H

- Layer thickness trend is highly similar among the experiments

- Volume of deepest layer remains nearly constant over time

Interior mass distribution is not unduly dependent upon either the mixed layer architecture or the choice of isopycnic or hybrid coordinates

Fixed-coordinate experiment: EXP-Hp

- Loses nearly all of the densest (and coldest) water in the domain over the 20-year period, as reflected in greater increase in heat content in comparison to the σ_θ experiments

σ_2 experiments: EXP-H σ_2 , EXP-H σ_2^*

- Smaller temporal changes in water mass distribution than in the σ_θ experiments

- Basin-averaged thickness of the 5 deepest layers remains relatively constant over 20 years

- Basin-averaged heat content decreases slightly over time in EXP-H σ_2 and remains relatively steady in EXP-H σ_2^* (the experiment with thermobaricity), in contrast to the increasing heat content of the σ_θ experiments

OVERTURNING/HEAT FLUX

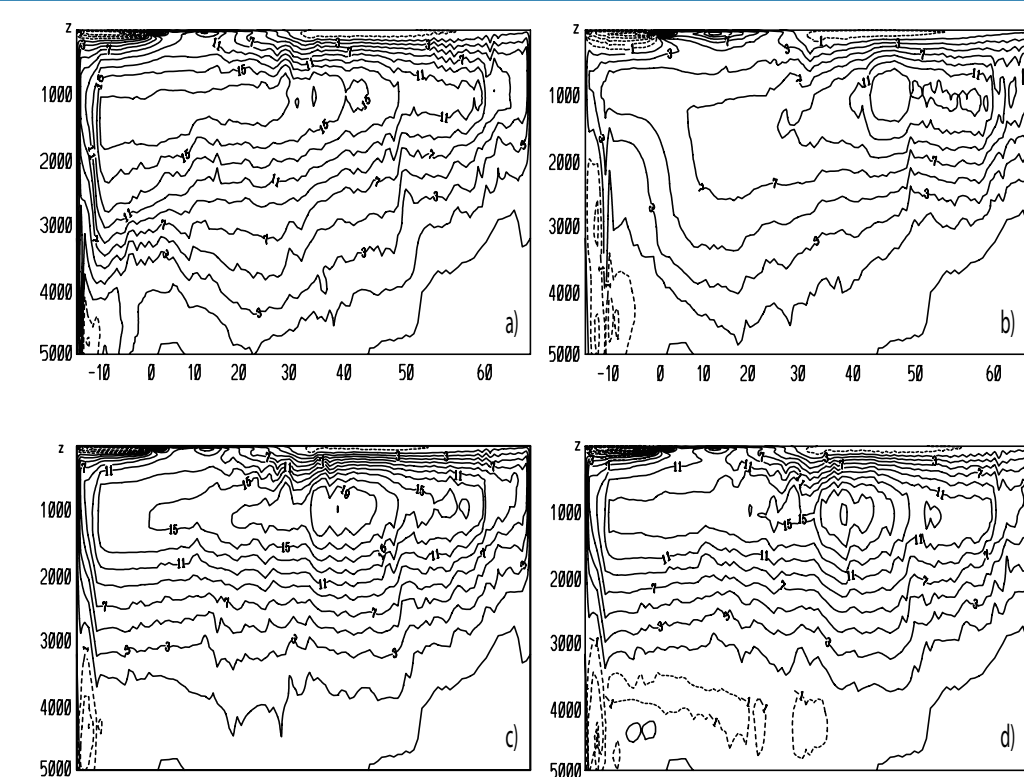


Fig. 8. Meridional overturning streamfunction, mean years 18-20, for (a) EXP-H, (b) EXP-Hp, (c) EXP-H σ_2 , (d) EXP-H σ_2^* . Contour interval 2 Sv; the zero contour is not shown. Dashed contours indicate negative values.

MERIDIONAL OVERTURNING

EXP-H_p (pressure-level coordinates) displays smaller maximum overturning and deeper southward transport than the hybrid experiments EXP-H, EXP-H σ_2 , and EXP-H σ_2^*

EXP-H σ_2 and EXP-H σ_2^* overturning streamfunctions are quantitatively similar to that of the σ_θ -coordinate EXP-H, but the overturning patterns differ significantly:

- Dense water flows south at shallower depths in EXP-H σ_2 and EXP-H σ_2^* than in EXP-H

- Circulation below 2000 m is weaker in the two σ_2 experiments due to the northward intrusion of AABW (not present in the σ_θ vertical discretization)

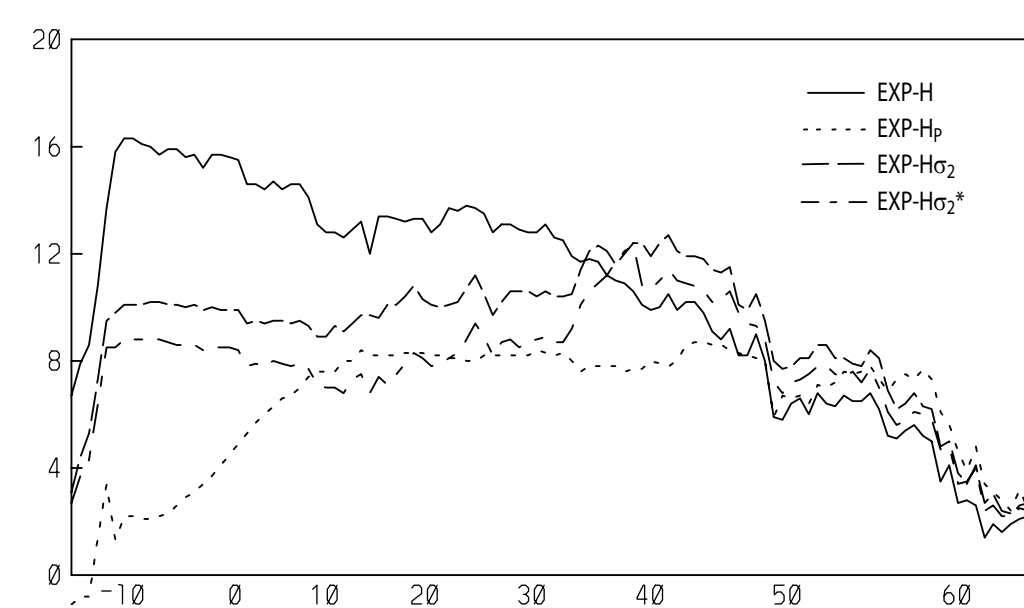


Fig. 9. Meridional overturning streamfunction values below 2000 m, mean years 18-20. Vertical axis in Sv. Black: EXP-D; long dash: EXP-E; dash-dot: EXP-F; dot: EXP-Dx.

MERIDIONAL HEAT TRANSPORT

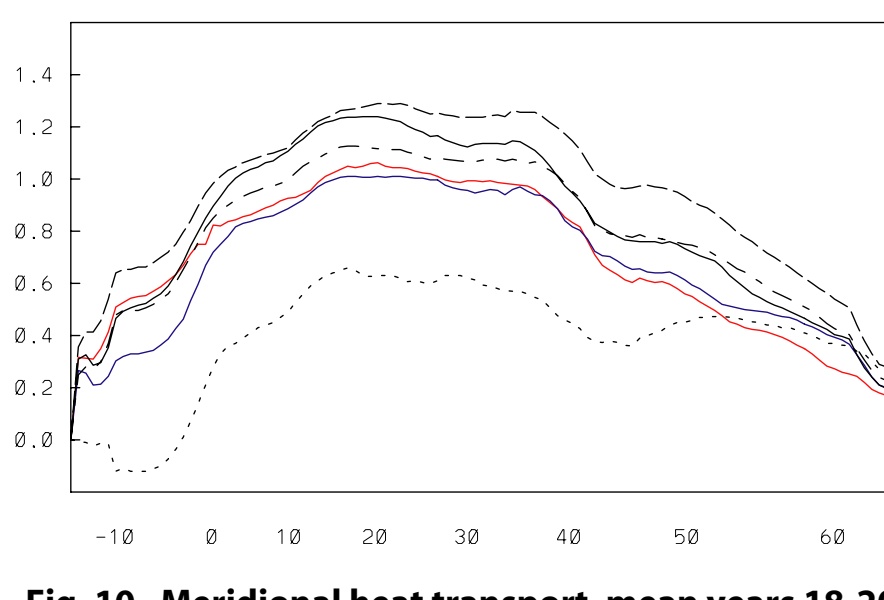


Fig. 10. Meridional heat transport, mean years 18-20. Vertical axis in PW. Red: EXP-M; blue: EXP-HKT; black: EXP-H; long dash: EXP-H σ_2 ; dash-dot: EXP-H σ_2^* ; dot: EXP-Hp.

EXP-H_p, with pressure-level coordinates, exhibits lowest heat transport values of all experiments

Hybrid experiments with KPP mixed layer (EXP-H σ_2 , EXP-H, EXP-H σ_2^*) have higher heat transport than those with K-T mixed layer (EXP-H_{KT}, EXP-M)

DEEP WATER TRANSPORT

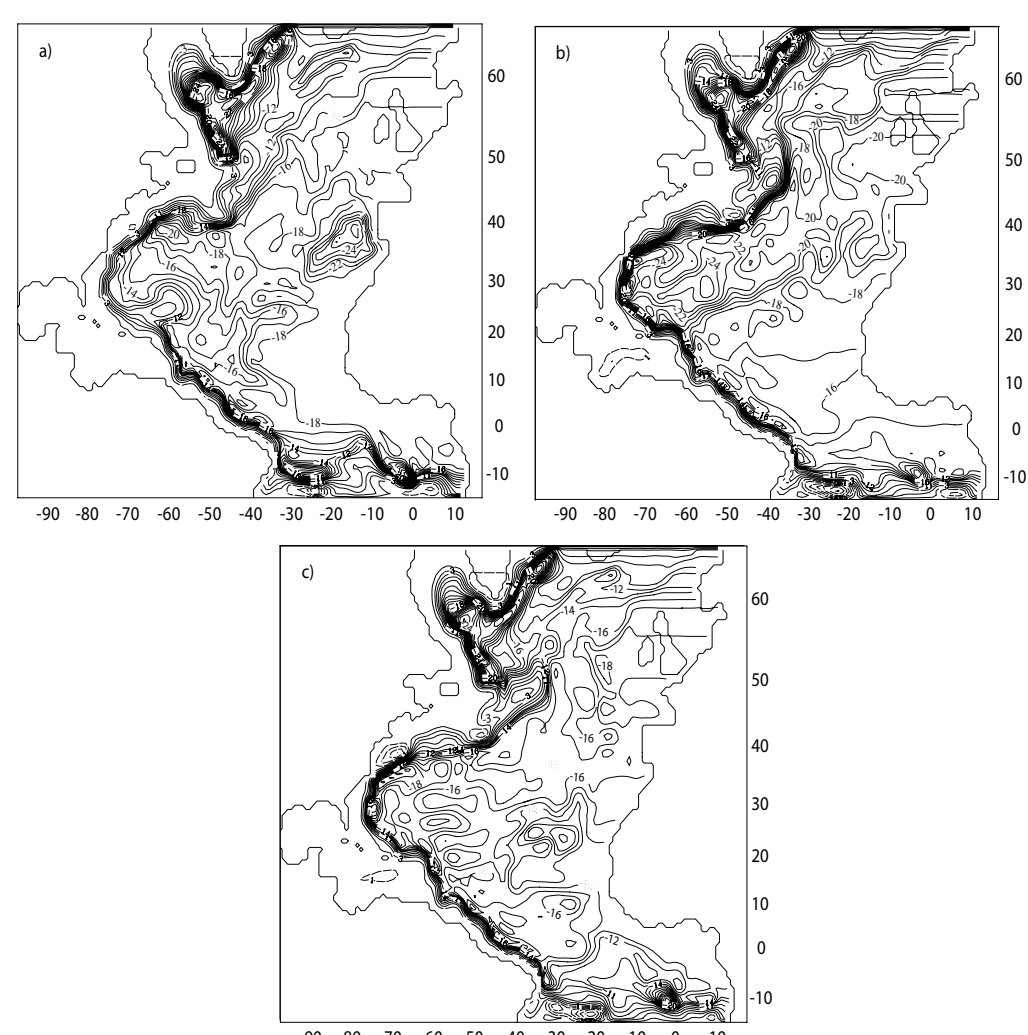


Fig. 11. Streamfunction for "lower deep" water masses ($\sigma_0 > 27.8$), mean years 18-20. (a) EXP-H, (b) EXP-H σ_2 , (c) EXP-H σ_2^* . Contour interval 1 Sv.

DEEP WATER MASS TRANSPORT

EXP-H σ_2 exhibits stronger circulation in deep ocean and more intense DWBC than EXP-H or EXP-H σ_2^* , as was the case for the surface circulation

Pressure gradients at the surface and in the deep ocean are modified to take thermobaricity into account in EXP-H σ_2^* , so that the AABW northward transport is represented in the interior circulation south of 20°N

Acknowledgements

This work has been supported by the National Ocean Partnership Program (NOPP) under Award # N00014-99-1-1066. The authors thank Dr. Ge Peng for making the poster and Jean Carpenter for redrafting the figures.

SUMMARY

Single-coordinate experiments (isopycnic, pressure-level) and hybrid experiments (σ_θ , σ_2 , σ_2^*) show that the concept of a generalized (hybrid) coordinate ocean model is viable.

The main difference between the σ_θ and σ_2 experiments is the model's representation of AABW. There is no distinct water mass representing AABW in the σ_θ discretization. However, the density structure of the AABW is well represented when a reference pressure of 20 MPa (~2000 m) is selected.

The differences between the σ_2 and σ_2^* experiments illustrate the importance of the thermobaricity. Without inclusion of the thermobaric effects, the pressure gradient above and below 2000 m does not take into account the modulation of seawater compressibility by potential temperature anomalies. Both the surface and deep circulation are much stronger in the experiment without thermobaricity. It is also only in the σ_2 experiment that the AABW can be seen flowing north along the eastern side of the domain.

REFERENCES

- Bleck, R., 2002: An oceanic general circulation model framed in hybrid isopycnic-cartesian coordinates. *Ocean Modelling*, 4, 55-88.
- Bryan, F. O., and W. R. Holland, 1989: A high resolution simulation of the wind- and thermohaline-driven circulation in the North Atlantic Ocean. In *Parameterization of Small-Scale Processes*, Proceedings of the Hawaiian Winter Workshop, Univ. of Hawaii, January 17-20, 1989, F. Muller and D. Anderson, Eds.
- Chassignet, E. P., H. Arango, D. Dietrich, T. Ezer, M. Ghil, D. B. Haidvogel, C.-C. Ma, A. Mehra, A. M. Paiva, and Z. Sirkes, 2000: DAMEE-NAB: The base experiments. *Dyn. Atmos. Oceans*, 32, 155-184.
- Chassignet, E. P., L. T. Smith, R. Bleck, and F. O. Bryan, 1996: A model comparison: Numerical simulations of the North and Equatorial Atlantic oceanic circulation in depth and isopycnic coordinates. *J. Phys. Oceanogr.*, 26, 1849-1867.
- Han, Y.-J., 1984: A numerical model ocean general circulation model. Part II: A baroclinic experiment. *Dyn. Atmos. Oceans*, 8, 141-172.
- Hellerman, S., and M. Rosenstein, 1983: Normal monthly wind stress over the world ocean with error estimates. *J. Phys. Oceanogr.*, 13, 1093-1104.
- Kraus, E. B., and J. S. Turner, 1967: A one-dimensional model of the seasonal thermocline: II. The general theory and its consequences. *Tellus*, 19, 98-106.
- Large, W. G., J. C. McWilliams, and S. C. Doney, 1994: Oceanic vertical mixing: a review and a model with a nonlocal boundary layer parameterization. *Rev. Geophys.*, 32, 363-403.
- Large, W. G., G. Danabasoglu, S. C. Doney, and J. C. McWilliams, 1997: Sensitivity to surface forcing and boundary layer mixing in a global ocean model: Annual-mean climatology. *J. Phys. Oceanogr.*, 27, 2418-2447.
- Levitus, S., 1982: *Climatological Atlas of the World Ocean*. NOAA Prof. Paper 13, 173 pp.
- Marsh, R., M. J. Roberts, R. A. Wood, and A. L. New, 1996: An intercomparison of a Bryan-Cox type ocean model and an isopycnic ocean model. Part II: The subtropical gyre and heat balances. *J. Phys. Oceanogr.*, 26, 1528-1551.
- Roberts, M. J., R. Marsh, A. L. New, and R. A. Wood, 1996: An intercomparison of a Bryan-Cox type ocean model and an isopycnic ocean model. Part I: The subpolar gyre and high-latitude processes. *J. Phys. Oceanogr.*, 26, 1495-1527.
- Smith, L. T., E. P. Chassignet, and R. Bleck, 2000: The impact of lateral boundary conditions and horizontal resolution on North Atlantic water mass formations and pathways in an isopycnic coordinate ocean model. *J. Phys. Oceanogr.*, 30, 137-159.

Contact Information

Prof. Eric Chassignet
(305) 361 - 4041
echassignet@rsmas.miami.edu